Microporous and Mesoporous Materials 205 (2015) 65–69

Contents lists available at ScienceDirect

Microporous and Mesoporous Materials

journal homepage: www.elsevier.com/locate/micromeso

NMR relaxation and exchange in metal–organic frameworks for surface area screening

Joseph J. Chen [a,*], Jarad A. Mason [b], Eric D. Bloch [b], David Gygi [b], Jeffrey R. Long [b,c], Jeffrey A. Reimer [a]

[a] Department of Chemical and Biomolecular Engineering, University of California, Berkeley, CA 94720, United States
[b] Department of Chemistry, University of California, Berkeley, CA 94720, United States
[c] Materials Sciences Division, Lawrence Berkeley National Laboratory, Berkeley, CA 94720, United States

ARTICLE INFO

Article history:
Received 2 May 2014
Accepted 14 July 2014
Available online 7 August 2014

Keywords:
Metal–organic frameworks
NMR relaxometry
Exchange
High-throughput screening

ABSTRACT

We describe a robust screening technique that correlates the surface area of metal–organic frameworks to the proton T_2 relaxation behavior of imbibed solvent at low field (13 MHz). In frameworks with small pore sizes (<1 nm) or strong solvent-framework interactions, diffusional exchange between the pore-confined and inter-particle solvent populations remains slow compared to the T_2 of the pore-confined solvent, allowing for a direct porosity analysis of the T_2 spectrum obtained from Laplace inversions. Increases in framework pore-size (>1 nm) lead to corresponding increases in the rate of solvent exchange, as confirmed by T_2 relaxation exchange (REXSY) experiments; increases in the pore size also increases the T_2 of the pore-confined solvent. The combination of these two effects results in comparable rates of relaxation and exchange, which precludes the direct analysis of Laplace inversions. Thus, two- and three-site kinetics models were applied to extract porosity from relaxation decays, thereby improving the utility of the porosity screening tool.

1. Introduction

Metal–organic frameworks are porous crystalline solids consisting of networks of metal clusters or ions connected by organic linkers through coordination bonds. The effectively infinite number of metal–ligand combinations and the modular nature of framework synthesis make high-throughput synthesis an effective optimization tool [1–6], but subsequent characterization of frameworks presents a bottleneck to this workflow. In a previous study we described a porosity-screening technique using nuclear magnetic resonance (NMR) relaxometry. This technique greatly simplified the necessary sample preparation for porosity analysis and reduced the measurement time, thus allowing for faster porosity characterization compared to a typical Brunauer–Emmett–Teller (BET) adsorption experiment [7]. The rate of transverse (T_2) relaxation in a variety of solvent-imbibed metal–organic frameworks and zeolites correlated directly to the two pore-size regimes formed by packed porous particles: nanometer-sized pores belonging to the inherent structure of the framework (pore-confined) and micron-sized voids between the individual crystallites (inter-particle). The clear delineation between the relaxation times of the pore-confined molecules ($\sim 10^{-2}$ to 10^{0} ms) and the inter-particle molecules ($\sim 10^{0}$ to 10^{3} ms) indicated that exchange between the two populations occurred slowly compared to the timescale of relaxation. Thus, the corresponding peak areas for each population, which are proportional to the number of molecules in each population, were directly analyzed to yield an NMR-derived porosity that strongly correlated to the BET surface area.

Direct analysis of the relaxation distributions hinges upon the ability to clearly distinguish the relaxation times of the pore-confined and inter-particle solvent. Diffusional exchange between the two results in relaxation distributions that no longer reflect the size of each population, and in the limiting case of fast exchange, the observed relaxation time is a weighted average of each population's relaxation rates [8–11]. Thus, the limitations of direct analysis depend on the relative magnitudes of the diffusion length and the particle size since solvent molecules that remain within the porous particle during the timescale of the experiment do not exchange with the inter-particle molecules. This direct analysis is also limited by the inherent difference in relaxation times between the pore and inter-particle populations, as well as by the resolution limits of the Laplace inversion algorithm used to deconvolute multi-exponential signals [12]. Given that the relaxation time of pore-confined molecules scales roughly with the pore radius, frameworks with larger pores (>1 nm) would likely exhibit longer pore relaxation times. Furthermore, larger pores

* Corresponding author.

http://dx.doi.org/10.1016/j.micromeso.2014.07.037
1387-1811/

would decrease the restrictions on diffusion within the framework, resulting in faster exchange. Because of these limitations, the "direct analysis" method was constrained to frameworks with BET surface areas of approximately 1700 m^2/g or less (<1 nm pore sizes). Many important frameworks possess pore sizes greater than 1 nm, since in microporous media (<2 nm pore size), pore volume, porosity, and surface area are proportional to pore size. Thus, the constraint on pore size greatly limits the utility of the technique. Notably, the M_2(dobdc) (MOF-74, dobdc^{4-} = 2,5-dioxido-1,4-benzenedicarboxylate, M = Mg, Ni, Co, Zn) family of frameworks tested in the previous study were also analyzed using the direct analysis method even though they possess pore sizes of ~1.4 nm [13,14]. In these frameworks, strong binding to the high density of open metal sites would greatly hinder diffusion, and thus, the relaxation signals would also exhibit a clear distinction between pore-confined and interparticle solvent.

Here, we describe a second analysis method that allows for the evaluation of high-porosity, large-pore metal organic frameworks and therefore expands the utility of the porosity screening tool. This method accounts for simultaneous relaxation and exchange by using kinetics models to fit the multi-exponential relaxation decays. The fitting results reveal that large-pore frameworks exhibit longer pore relaxation times and faster exchange compared to the frameworks previously tested. Pore volumes derived from these fits correlate strongly with the Langmuir surface area for frameworks up to ~5000 m^2/g, thus allowing for a significant increase in the testing range of the NMR porosity screening tool.

2. Experimental

The compound 4,4″-dihydroxy(1,1′:4′,1″-terphenyl)-3,3″-dicarboxylic acid (H_4dotpdc) was synthesized as detailed in the Supporting information. All other reagents were obtained from commercial vendors and used without further purification. Infrared spectra were obtained on a Perkin-Elmer Spectrum 100 Optica FTIR spectrometer furnished with an attenuated total reflectance accessory. Diffraction data were collected with 0.02° steps using a Bruker AXS D8 Advance diffractometer equipped with Cu-Kα radiation (λ = 1.5418 Å), a Göbel mirror, a Lynxeye linear position-sensitive detector, and mounting the following optics: fixed divergence slit (0.6 mm), receiving slit (3 mm), and secondary beam Soller slits (2.5°). The generator was set at 40 kV and 40 mA.

Gas adsorption isotherms were measured using a Micromeritics ASAP 2020 instrument. For standard measurements in ASAP low-pressure glass sample holders, activated samples were transferred under a N_2 atmosphere to preweighed analysis tubes, which were capped with a Transeal. The samples were evacuated on the ASAP until the outgas rate was less than 3 μbar/min. The evacuated analysis tubes containing degassed samples were then carefully transferred to an electronic balance and weighed to determine the mass of sample (typically 100–200 mg). The tube was fitted with an isothermal jacket and transferred back to the analysis port of the gas adsorption instrument. The outgas rate was again confirmed to be less than 3 μbar/min. Langmuir surface areas were determined by measuring N_2 adsorption isotherms in a 77 K liquid N_2 bath and calculated using the Micromeritics software, assuming a value of 16.2 $Å^2$ for the molecular cross-sectional area of N_2.

2.1. Synthesis of Sc-MIL-100

The compound Sc-MIL-100 was synthesized by following the published procedure [15]. The successful synthesis and activation of the framework was confirmed by comparing the X-ray powder diffraction pattern and Langmuir surface areas to those previously reported.

2.2. Synthesis of Fe-MIL-100

The compound Fe-MIL-100 was synthesized by following the published procedure [16]. The successful synthesis and activation of the framework was confirmed by comparing the X-ray powder diffraction pattern and Langmuir surface areas to those previously reported.

2.3. Synthesis of Al(OH)(bpdc)

The compound Al(OH)(bpdc) was synthesized by following the published procedure [17]. The successful synthesis and activation of the framework was confirmed by comparing the X-ray powder diffraction pattern and Langmuir surface areas to those previously reported.

2.4. Synthesis of MOF-5

The compound MOF-5 was synthesized and activated using a strategy adopted from a previous report [18]. Specifically, H_2bdc (0.66 g, 4.0 mmol), $Zn(NO_3)_2{\cdot}6H_2O$ (3.6 g, 12 mmol), and *N*,*N*-diethylformamide (DEF, 100 mL) were combined in a 250-mL Schlenk flask sealed with a rubber septum. The Schlenk flask was heated at 90 °C for 24 h, then placed under N_2, and the reaction solvent was removed via cannula and replaced with anhydrous *N*, *N*-dimethylformamide (DMF) at room temperature. The DMF was exchanged with fresh, anhydrous DMF two further times. The DMF was then exchanged with anhydrous dichloromethane (DCM) at room temperature. The DCM was exchanged with fresh, anhydrous DCM two further times, then the majority of the DCM was removed via cannula. The resulting clear, cubic crystals were activated by heating at 150 °C under vacuum for 24 h. The successful synthesis and activation of the framework was confirmed by comparing the X-ray powder diffraction pattern and Langmuir surface areas to those previously reported.

2.5. Synthesis of Co_2(dotpdc)

The compound Co_2(dotpdc) (dotpc^{4-} = 4,4″-dihydroxy(1,1′:4′,1″-terphenyl)-3,3″-dicarboxylate) was synthesized by following the published procedure. The successful synthesis and activation of the framework was confirmed by comparing the X-ray powder diffraction pattern and Langmuir surface areas to those previously reported [19].

2.6. Framework solvent exchange

Evacuated metal–organic framework samples were imbibed by soaking the framework in DMF overnight. The MOFs were then filtered and dried in a N_2 atmosphere to evaporate excess solvent. Subsequent thermogravimetric analysis (TGA Q50, TA Instruments, New Castle, DE) was used to quantify solvent content of the solvent-filled MOF. Solvent content was determined from the mass loss prior to degradation temperatures for each material. Solvent content was normalized to the dry weight of the MOF sample, and was systematically varied by micropipette addition or thermal evaporation.

2.7. NMR Experiments

^{1}H-NMR relaxation was measured using a 13 MHz Aster Enterprises permanent magnet equipped with a homebuilt probe. This probe consisted of a simple solenoid coil with a diameter of ~8 mm wired to tuning and matching capacitors. A Kea II spectrometer was used for pulse generation and signal acquisition, and all pulse programs were written using a Prospa v3.11 software

package. Carr-Purcell-Meiboom-Gill (CPMG) pulse sequences [20,21] were used to measure the T_2 relaxation, while T_2–T_2 relaxation exchange experiments (REXSY) were used to qualitatively identify the presence of exchange [8–11]. All samples were measured at room temperature.

A fast Laplace inversion numerical algorithm from Magritek was used to generate 1D and 2D relaxation distributions [22], and the kinetics model fits (see below) were conducted using a nonlinear least-squares fitting program. To verify the quality of the fit, the p-value of the residuals was calculated, and a criterion of $p < 0.01$ was used to reject the fit. In order to overcome local minima randomly selected starting points were used to fit the data, though all starting points eventually converged to the same fitting values. The fits were also rejected if the fitted values, especially the pore-confined relaxation time, exhibited an especially large deviation, indicating that the fit was no longer sensitive to the pore-confined solvent. This situation often occurred at high solvent contents where the signal from the pore-confined solvent was small.

3. Results and discussion

The relaxation distributions are shown in Fig. 1 for Al(OH)(bpydc) (MOF-253; $bpydc^{2-}$ = 2,2′-bipyridine-5,5′-dicarboxylate), a high porosity framework ($SA_{Langmuir}$ = 2250 m^2/g) [17], imbibed with *N*,*N*-dimethylformamide (DMF) at various solvent contents. These relaxation distributions qualitatively differ from those seen previously [7], with no clear indication of pore-confined and bulk solvent, especially considering the changes in the relaxation distribution with increasing solvent content. Given the pore volume of Al(OH)(bpydc) (0.89 cm^3/g) [17], full loading of the pore volume with DMF (0.948 g/cm^3) should occur at approximately 0.8 mL/g. Assuming that solvent molecules would preferentially adsorb into the pores first, a single relaxation population representing pore-confined solvent should be observed at these loadings, and this behavior was observed in the small-pore frameworks tested previously [7]. However, at the lowest solvent loading (0.8 mL/g), three distinct peaks are observed at ~0.3 ms, ~1.5 ms, and ~12 ms, indicating that there are multiple relaxation populations present. As solvent is added, all of the peak areas change, some of the peaks appear to coalesce, and there is a general shift to longer relaxation times. This behavior again contrasts with that seen in small-pore frameworks, where addition of solvent would cause a clearly-separated second relaxation population to appear. This population corresponded to the inter-particle solvent, allowing for direct porosity analysis. Thus, the divergent relaxation behavior of large-pore frameworks, which is seen in a variety of other tested frameworks (i.e. Sc-MIL-100, Fe-MIL-100, MOF-5, and Co_2(dotpdc), a terphenyl-based expanded analogue of Mg_2(dobpdc) featuring coordinatively unsaturated Co^{2+} cation sites [23]), precludes the direct interpretation of the distributions.

We performed 2D T_2–T_2 relaxation exchange (REXSY) experiments to investigate the origin of this divergent relaxation behavior, as exchange between relaxation populations can create effects very similar to those seen in Fig. 1 [8–11]. The 2D T_2–T_2 relaxation maps produced from the Laplace inversion of the data can help identify the presence of exchange. Although the populations shown in these maps are subject to many of the same effects as those seen in the 1D relaxation distributions, any populations appearing off the diagonal (Fig. 2) are strong indicators of exchange processes. The T_2–T_2 map for MOF-253 measured at high solvent content (2.8 mL/g) for an exchange time of 10 ms is shown in Fig. 2. The exchange map qualitatively indicates that exchange is indeed happening at a timescale of $1/k \sim 10$ ms, where k is the exchange rate, as indicated by the presence of populations off the diagonal line. This implies that the exchange processes occur at a rate comparable to the relaxation rate, a situation where the relaxation distributions are strongly affected by the exchange processes. Though exchange processes would skew the peak areas and positions, the exchange peaks suggest the presence of three populations at roughly distinguishable relaxation times: short (~0.4 ms), intermediate (~4 ms), and long (>10 ms). Furthermore, exchange peaks appear for exchange between the short and intermediate relaxation populations as well as between the intermediate and long relaxation populations, but not between the short and long relaxation populations. In our previous work, we identified the short, intermediate, and long relaxation populations as the pore-confined, interfacial, and inter-particle solvent, respectively. Since the pore-confined solvent and the inter-particle solvent must exchange through the interfacial layer outside the porous particles, the exchange peaks suggest that the three populations seen in the T_2–T_2 map can also be assigned as before. Finally, these exchange experiments allow us to speculate on the pore diffusion coefficient. The solvent diffusion coefficient within the framework pores should be greatly decreased from the neat solvent due to the effect of pore confinement, and thus, the exchange between pore-confined and interfacial solvent would be governed by the rate-limiting pore diffusion process. As a first assumption we assume that the diffusion length must be roughly on the order of the particle size, which results in significant mixing of populations and in skewed relaxation distributions. Given a particle size on the order of 1 μm and an exchange time of 1–10 ms, the pore diffusion coefficient would be on the order of 10^{-10} to 10^{-11} m^2/s. Though

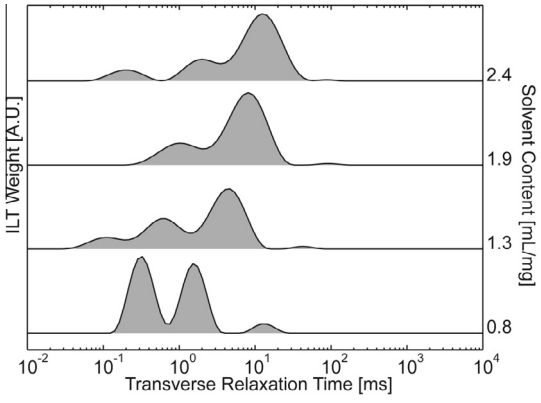

Fig. 1. Transverse (T_2) relaxation distributions of Al(OH)(bpydc) with various amounts of DMF added. The total intensity at each solvent content is normalized to unity.

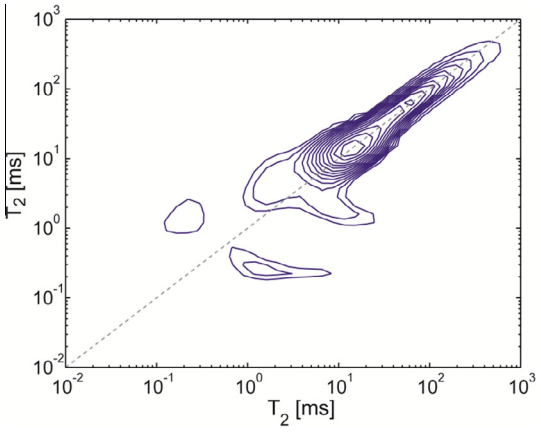

Fig. 2. Contour plot of the T_2–T_2 relaxation map for Al(OH)(bpydc) at high loading (2.8 mL/g) with an exchange time of 10 ms. The dashed line indicates the diagonal ($T_2 = T_2$).

self-diffusion coefficient measurements for large, polar molecules, such as DMF, in microporous media are largely unavailable, the diffusion coefficients estimated here are not unreasonable given the literature available for alcohol diffusion in faujasite-type zeolites and zeolitic imidazolate frameworks (ZIFs) [24,25].

In order to quantify the relaxation and exchange processes between the pore-confined (A), interfacial (B), and inter-particle (C) populations, we used a three-site kinetics model to fit the 1D relaxation data:

$$\frac{\partial M_a}{\partial t} = -r_a M_a - k_{ab} M_a + k_{ba} M_b \quad (1)$$

$$\frac{\partial M_b}{\partial t} = -r_b M_b + k_{ab} M_a - k_{ba} M_b + k_{cb} M_c - k_{bc} M_b \quad (2)$$

$$\frac{\partial M_c}{\partial t} = r_c M_c - k_{cb} M_c + k_{bc} M_b \quad (3)$$

$$M_{a,b,c}(t = 0) = M^0_{a,b,c} \quad (4)$$

Here, M_i represents the magnetization of each population, r_a is the inherent relaxation rate of each population, and k_{ij} is the exchange rate of population i to population j. Note that $k_{ac} = k_{ca} = 0$, indicating that the pore-confined and inter-particle populations do not exchange directly. Due to mass balance, only two independent exchange coefficients remain, and the rates of A–B exchange and B–C exchange can be described by a single variable each. Also, though the 2D relaxation data could also be fitted using this model, the 1D fit yielded nearly identical results, rendering the 2D fits superfluous. The pore volume was taken as the initial magnetization of the pore-confined solvent (M^0_a). The model fits for Al(OH)(bpydc) (see Fig. 3) indicate that the pore volume and pore relaxation time $T_{2,\text{pore}} = 1/r_a$ increase with increasing solvent content, which suggests that the pores are filling as solvent is added. In frameworks with pore sizes much larger than the solvent molecule diameter, the framework walls are fully covered by solvent molecules at high adsorbate loadings, and adsorption of any additional solvent molecules would be akin to a condensation process. In this case, adsorption in the inter-particle space and in the framework pores would exhibit similar heats of adsorption (i.e. BET-like adsorption), resulting in growth of both the pore-confined and inter-particle solvent population with increasing solvent content. This effect was unanticipated and would also result in differing relaxation distributions when compared to that for small-pore frameworks. Also, for all solvent contents, the exchange time between the pore-confined and interfacial solvent ($1/k_a$) is on the order of 1–10 ms, with the exchange time increasing for increasing solvent contents. These values agree with those estimated from the qualitative analysis of the T_2–T_2 map. Note that at the highest solvent content, both values display an incommensurately large increase in values, an artifact indicating that the least-squares algorithm is no longer sensitive to the proportionally small signal stemming from the pore-confined solvent. The resulting fits from these data were disregarded. Since sensitivity to the pore-confined solvent population is lost at higher solvent contents, the pore volume at the highest solvent content with an acceptable fit was taken as an estimate of the actual pore volume. This algorithm was applied to the relaxation data for four additional large-pore, high-porosity frameworks (Sc-MIL-100, Fe-MIL-100, Co_2(dotpdc), and MOF-5). The relaxation data from our previous study [7] was also analyzed using a two-site kinetics model for comparison; the choice of a two-site model rather than a three-site model stemmed from the relaxation data exhibiting largely bimodal behavior (see Supporting information). The model-derived pore volume (see Fig. 4) agrees well with the Langmuir surface areas for both the two- and three-site model fits, indicating that the model is largely accounting for the physics of relaxation and exchange in large-pore frameworks. Also, the pore volumes derived from the two-site kinetics model fit to the previously obtained relaxation data are nearly equal to those calculated from the original analysis of the relaxation distributions, further confirming the validity of this new analysis method. By using this method, frameworks with larger surface areas can be characterized, thereby improving the utility of an NMR relaxometry-based porosity screening tool.

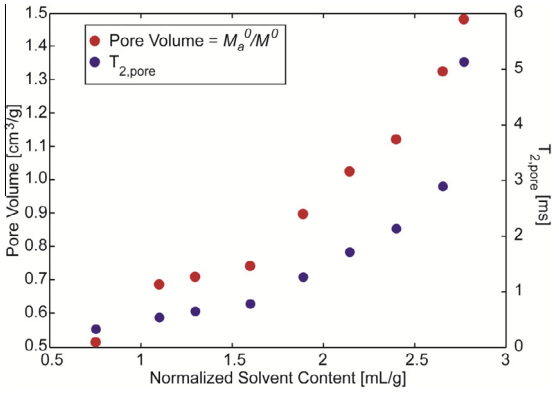

Fig. 3. Pore volume (M^0_a) and $T_{2,\text{pore}}$ ($1/r_a$) resulting from the fits of the three-site kinetics model to the relaxation data for Al(OH)(bpydc). Note that the points at the highest solvent content were disregarded due to poor fitting ($p < 0.01$) and an incommensurate increase in both values.

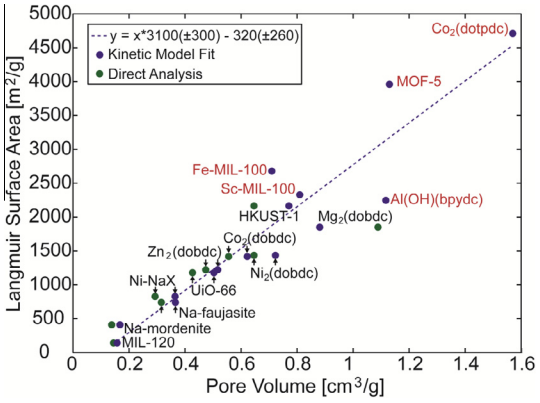

Fig. 4. Correlation of Langmuir surface area to the model-derived pore volume. Dashed lines indicate the linear fit to the kinetic model data. Note that the labels in red indicate the three-site model fits for data obtained on the homogeneous-field permanent magnet, and the labels in black indicate the two-site model fits for previously obtained data from the single-sided NMR-MOUSE. The pore volumes derived from the direct analysis method of the NMR-MOUSE data are shown in green [7]. The Langmuir surface areas for the frameworks used in the three-site model fits were determined from 77 K N_2 adsorption isotherms.

4. Conclusions

In this study, we describe a new analysis method to measure the surface area of high-porosity, large-pore metal-organic frameworks using NMR relaxometry. In these frameworks, the relaxation distributions do not reflect the actual porosity due to the diffusional exchange occurring on the timescale of relaxation. We applied kinetics models to account for simultaneous relaxation and exchange and derived a pore volume that correlates well to the surface area, though further work is needed to investigate the behavior of the model fits with increasing solvent content. Nevertheless, the ability to characterize frameworks with large surface areas greatly improves the utility of the relaxometry-based screening tool.

Acknowledgements

The information, data, or work presented herein was funded by the U.S. Department of Energy, Advanced Research Projects Agency – Energy (ARPA-E) under Grant No. DE- AR0000103. The authors acknowledge Dr. Kenji Sumida, and Ms. Mary Anne Manumpil for assistance with sample preparation. We also thank NSF for providing graduate fellowship support for J.A.M.

Appendix A. Supplementary data

Supplementary data associated with this article can be found, in the online version, at http://dx.doi.org/10.1016/j.micromeso.2014.07.037.

References

[1] R. Banerjee, A. Phan, B. Wang, C. Knobler, H. Furukawa, M. O'Keeffe, O.M. Yaghi, Science 319 (2008) 939–943.
[2] E. Biemmi, S. Christian, N. Stock, T. Bein, Micropor. Mesopor. Mater. 117 (2009) 111–117.
[3] N. Stock, T. Bein, Angew. Chem. Int. Ed. 43 (2004) 749–752.
[4] K. Sumida, S. Horike, S.S. Kaye, Z.R. Herm, W.L. Queen, C.M. Brown, F. Grandjean, G.J. Long, A. Dailly, J.R. Long, Chem. Sci. 1 (2010) 184–191.
[5] C. Volkringer, T. Loiseau, N. Guillou, G. Férey, M. Haouas, F. Taulelle, E. Elkaim, N. Stock, Inorg. Chem. 49 (2010) 9852–9862.
[6] P. Maniam, N. Stock, Inorg. Chem. 50 (2011) 5085–5097.
[7] J.J. Chen, X. Kong, K. Sumida, M.A. Manumpil, J.R. Long, J.A. Reimer, Angew. Chem. Int. Ed. 52 (2013) 12043–12046.
[8] P. McDonald, J.P. Korb, J. Mitchell, L. Monteilhet, Phys. Rev. E 72 (2005).
[9] L. Monteilhet, J.P. Korb, J. Mitchell, P. McDonald, Phys. Rev. E 74 (2006).
[10] K. Washburn, P. Callaghan, Phys. Rev. Lett. 97 (2006) 175502.
[11] M. Van Landeghem, A. Haber, J.B. D'espinose De Lacaillerie, B. Blümich, Concepts Magn. Reson. Part A 36 (2010) 153–169.
[12] Y.Q. Song, L. Venkataramanan, L. Burcaw, J. Chem. Phys. 122 (2005) 104104.
[13] S.R. Caskey, A.G. Wong-Foy, A.J. Matzger, J. Am. Chem. Soc. 130 (2008) 10870–10871.
[14] P.D. Dietzel, B. Panella, M. Hirscher, R. Blom, H. Fjellvag, Chem. Commun. (2006) 959–961.
[15] Y.T. Li, K.H. Cui, J. Li, J.-Q. Zhu, X. Wang, Y.-Q. Tian, Chin. J. Inorg. Chem. 5 (2011) 951–956.
[16] P. Horcajada, S. Surblé, C. Serre, D.-Y. Hong, Y.-K. Seo, J.-S. Chang, J.-M. Greneche, I. Margiolaki, G. Férey, Chem. Commun. (Cambridge, UK) (2007) 2820–2822.
[17] E.D. Bloch, D. Britt, C. Lee, C.J. Doonan, F.J. Uribe-Romo, H. Furukawa, J.R. Long, O.M. Yaghi, J. Am. Chem. Soc. 132 (2010) 14382–14384.
[18] S.S. Kaye, A. Dailly, O.M. Yaghi, J.R. Long, J. Am. Chem. Soc. 129 (2007) 14176–14177.
[19] D. Gygi, E.D. Bloch, J.A. Mason, W.L. Queen, M.R. Hudson, A. Dailly, M. Beckner, C.M. Brown, J.R. Long, Hydrogen storage in the Metal–Organic Frameworks M2(dobpdc) (M = Mg, Mn, Fe Co, Ni, Zn), (in preparation).
[20] H. Carr, E. Purcell, Phys. Rev. 94 (1954) 630–638.
[21] S. Meiboom, D. Gill, Rev. Sci. Instrum. 29 (1958) 688–691.
[22] L. Venkataramanan, Y.Q. Song, M.D. Hurlimann, IEEE Trans. Signal Process. 50 (2002) 1017–1026.
[23] T.M. McDonald, W.R. Lee, J.A. Mason, B.M. Wiers, C.S. Hong, J.R. Long, J. Am. Chem. Soc. 134 (2012) 7056–7065.
[24] J. Kärger, D.M. Ruthven, D.N. Theodorou, Diffusion in Nanoporous Materials, Wiley-VCH, Weinheim, Germany, 2012.
[25] J.A. Gee, J. Chung, S. Nair, D.S. Sholl, J. Phys. Chem. C 117 (2013) 3169–3176.